THE ASTROPHYSICAL JOURNAL, 464:847–856, 1996 June 20

M1-46: A CASE STUDY ON MULTIPLE-SHELL PLANETARY NEBULA FORMATION

M. A. GUERRERO[1] AND A. MANCHADO[1]
Instituto de Astrofisica de Canarias, E-38200 La Laguna (Tenerife), Spain; mar@iac.es
L. STANGHELLINI
Osservatorio Astronomico di Bologna, I-40126 Bologna, Italy
AND
A. HERRERO
Instituto de Astrofisica de Canarias, E-38200 La Laguna (Tenerife), Spain
Received 1995 June 19; accepted 1996 January 8

ABSTRACT

We discuss in detail the evolutionary path of the multiple-shell planetary nebula M1-46, in the light of our new observations. The velocities of the halo and main nebula correspond to a dynamical time lap between the shells of about 6.8×10^4 yr. By means of a non-LTE analysis of the central star's spectrum, we derived a stellar temperature of $T_{\rm eff} = 45{,}000$ K, which, coupled to the visual magnitude and an appropriate bolometric correction, gives a stellar luminosity of 5370 $L_\odot$. The mass of the central star has been evaluated to be 0.6 $M_\odot$, and its interpulse time on the asymptotic giant branch is 7.6×10^4 yr. The agreement between the observed intershell time lap and the evolutionary interpulse time lap points to the fact that the formation of this planetary nebula could be ascribed to the gasping mass loss associated with the thermal pulses at the thermally pulsating asymptotic giant branch.

The high-resolution spatially resolved observations reveal the presence of different kinematical components in the main nebula which cannot be understood in a homogeneous expanding shell scenario.

As regards the chemical abundances, M1-46 has the typical abundances of a type II planetary nebula. No definite abundance gradient between the shells is found.

Subject headings: ISM: structure — planetary nebulae: individual (M1-46) — stars: AGB and post-AGB — stars: fundamental parameters

1. INTRODUCTION

Planetary nebulae (PNs) with multiple shells (Chu, Jacoby, & Arendt 1987; Balick et al. 1992) represent ideal laboratories for studying the final phases in the evolution of stars with *gasping* mass loss at the asymptotic giant branch (AGB), during the thermal pulses of the helium-shell (TP-AGB). Also, multiple-shell PNs are interesting for shedding some light on the gasdynamical evolution of post-AGB (P-AGB) shells (Frank, Balick, & Riley 1990).

Frank, van der Veen, & Balick (1994) tried to correlate the intershell time lap of a set of these PNs with their interpulse timelap, calculated using the theoretical evolutionary tracks by Vassiliadis & Wood (1993, hereafter VW93), but they did not find a convincing correlation. Stanghellini & Pasquali (1995) realized that the two classes of multiple-shell PNs described by Chu et al. (1987), namely, type I or detached halo (DH) and type II or attached halo (AH) PNs, represent distinct evolutionary paths. In fact, for DH PNs intershell and interpulse time laps are within their respective errors, while for AH PNs no observational errors could be invoked to make these time laps comparable. Until now, the lack of a reliable database covering kinematic studies of the relative motion of the shells of PNs with high spectral resolution have prevented these kinds of studies.

With these premises in mind, we started a detailed kinematic study on the DH PN M1-46, a round and compact PN (14″ diameter) surrounded by a fainter limb-brightened halo (59″ diameter), according to the narrow-band imagery by Schwarz, Corradi, & Melnick (1992). A high-resolution long-slit spectrum was obtained in order to investigate the internal motion of the different shells and radial velocity of the whole nebula. In addition long-slit low-dispersion spectra were obtained to determine the physical conditions and chemical abundances of the ionized gas in this object and the stellar surface temperature.

In § 2 we describe the observations. The analysis of the kinematical properties from the echelle observations is dealt with in § 3, while in § 4 we study the physical properties and chemical abundances of the nebular material, as well as the properties of the central star. In § 5 we discuss the correlation between the central star's evolution and the formation of the multiple shell structure in M1-46. In § 6 we investigate the mass and mass-loss rate of each shell. Finally, a summary is given in § 7.

2. OBSERVATIONS

M1-46 was observed on 1993 August 7, with the 4.2 m William Herschel Telescope at the Roque de los Muchachos Observatory (La Palma, Spain), using the Utrecht Echelle Spectrograph (UES) with the 79 lines mm^{-1} echelle grating and a 700 mm focal length camera. The spatial scale on the detector, a Tektronix CCD (1024 × 1024 array with a pixel size of 24 μm), was 0.″36 $pixel^{-1}$, with a field of view on the sky of 200″. The slit width was equivalent to 1.″1; the reciprocal dispersion was 2.92 Å mm^{-1} (0.07 Å $pixel^{-1}$) at 6560 Å, and the instrumental FWHM was 6.9 ± 0.3 km s^{-1}, as deduced from calibration lamps. Observations were taken through a narrow-band filter which isolates the Hα and the [N II] λλ6548,6584 lines in the 34th echelle order.

[1] Visiting Astronomer, German-Spanish Astronomical Center, Calar Alto, operated by the Max-Planck-Institut für Astronomie, Heidelberg, jointly with the Spanish National Commission for Astronomy.

The long-slit low-dispersion spectra were secured with the Cassegrain Twin Spectrograph (CTS) on the 3.5 m telescope at Calar Alto (CAHA) Observatory (Almería, Spain) in 1993 July. This instrument includes two separate spectroscopic channels (blue and red) that allow intermediate spectral resolution data to be obtained from 3500 to 7350 Å operating simultaneously with two CCD detectors, one for each channel. We used two 1024 × 1024 Tektronix CCDs with a pixel size of 24 μm. The slit was 1".2 wide and up to 5' long. The blue T08 and red T04 grisms, both with 600 lines mm^{-1}, gave a reciprocal dispersion of 72 Å mm^{-1}. We achieved a spectral resolution of 3.5 Å and a spatial resolution of 0".96.

Spectroscopic observations are summarized in Table 1.

3. KINEMATIC PROPERTIES OF M1-46

The long-slit echelle observations allow the kinematical behavior of the different parts of this nebula to be investigated separately. In particular, expansion velocities of the main nebula and the halo, and the radial velocity of the whole nebula, can be computed. Figure 1 presents the UES long-slit spectrum of M1-46, in the form of a velocity-position plot, for the [N II] λ6584 (Fig. 1*a*) and Hα (Fig. 1*b*) lines. From Figure 1*a*, the velocity range of the main nebula extends over 50 km s^{-1}.

In order to calculate the expansion velocity of the main nebula with the highest possible accuracy, a spectrum at the central star's position was extracted (Fig. 2). Since the expansion detected in this aperture is supposed to be in the observer's line of sight, the velocity determination is not affected by geometric projections. The [N II] λ6584 line was used for computing the velocities rather than the Hα line, since the former line is strong enough and has a smaller thermal broadening than the latter. The adopted rest wavelength for these lines are 6583.37 Å and 6562.85 Å, respectively. Figure 3 shows a four-Gaussian fit and the residuals. The velocities, corrected for the local standard of rest, are presented in Table 2. The maximum velocity difference is

TABLE 1

ECHELLE OBSERVATIONS AND LOW-RESOLUTION SPECTROSCOPY OF M1-46

Telescope and Instrument	Spectral Range (Å)	Dispersion (Å $pixel^{-1}$)	Offset from Central Star	Position Angle	Exposure Time (s)
4.2 m WHT (UES).....	6500–6600	0.07	0"	313°	900
3.5 m CAHA (TCS).....	3650–5250	1.76	0	313	600
3.5 m CAHA (TCS).....	5700–7350	1.77	0	313	300
3.5 m CAHA (TCS).....	3650–5250	1.76	13	313	2000
3.5 m CAHA (TCS).....	5700–7350	1.77	13	313	1800

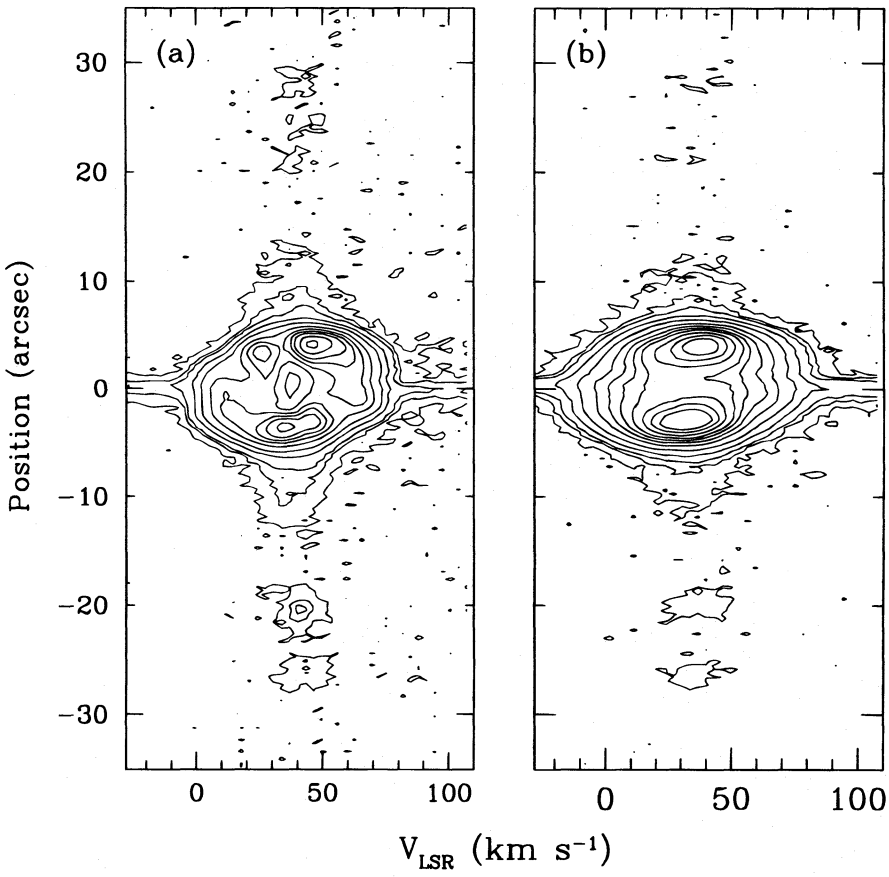

FIG. 1.—Contour maps of the long-slit echelle of the (*a*) [N II] λ6584 and (*b*) Hα lines. Contour levels are at 95%, 80%, 65%, 50%, 40%, 30%, 20%, 10%, 5%, 2%, 1.25%, and 0.5% of the peak value (3890 counts in [N II], 3275 counts in Hα).

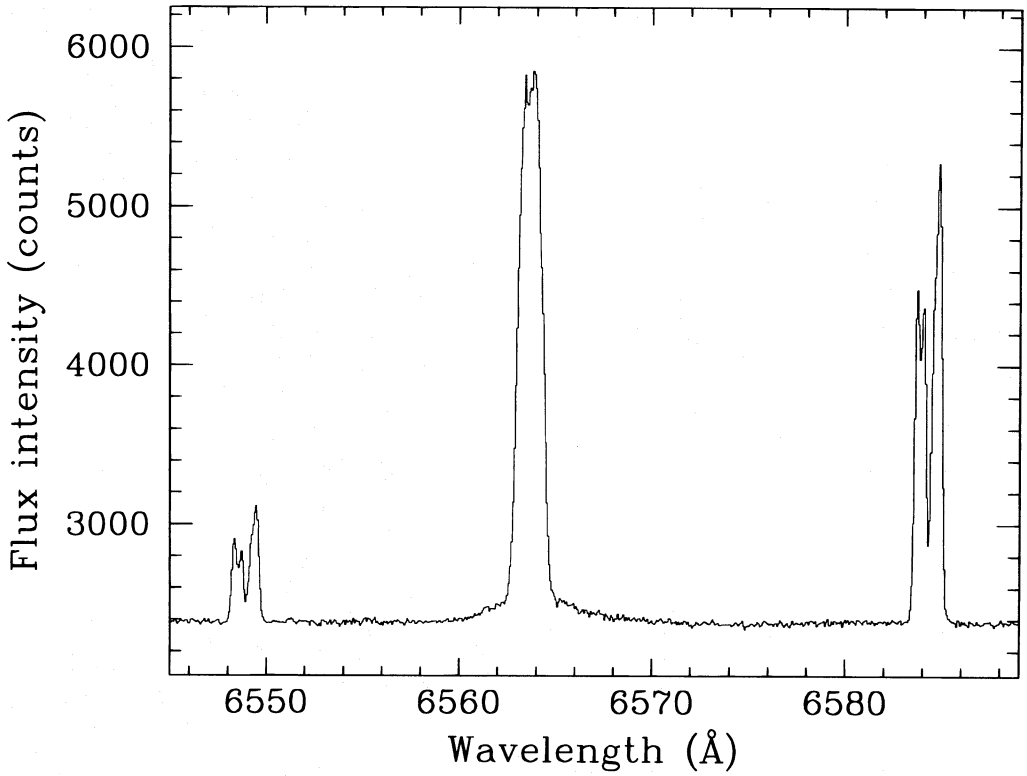

FIG. 2.—Hα and [N II] line profiles at the central position (N). The nitrogen lines are clearly split into multiples components, revealing that the kinematics of the shell are not straightforward. The Hα line is superimposed on a broad, stellar feature.

52.4 km s^{-1}, which can be interpreted as an expansion velocity of 26.2 km s^{-1}, while the difference between the velocities of the other two components is roughly half this value ($\Delta V_{exp}/2 = 11.8$ km s^{-1}). The radial velocity is 37 ± 1 km s^{-1}, close to the value (30 ± 3 km s^{-1}) obtained by Meatheringham, Wood, & Faulkner (1988).

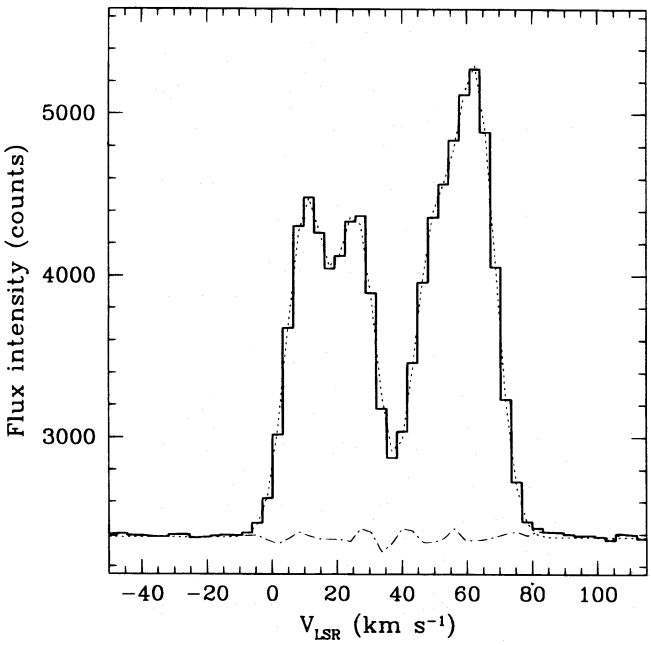

FIG. 3.—Four Gaussian fits (*dotted line*) to the [N II] λ6584 profile at the nuclear position (*solid line*). The residuals are also shown (*dot-dashed line*). The FWHM was 0.30 Å for all the components.

The FWHM, ~14 km s^{-1}, exceeds the instrumental FWHM; this is caused by the convolution of thermal and turbulent components (including possible bulk motion). A faint feature was detected at $\lambda \sim 6579$ Å extending spatially along the main nebula (it cannot be seen in Fig. 1 because it is very faint compared to the stellar continuum at this position). We identified this line as C II λ6578. Presumably the associated line C II λ6583 is present, but we estimated this to be too faint (~0.3% the intensity of [N II] λ6583) to introduce an appreciable error.

The detection of four distinct components (Fig. 3) was unpredicted, if we consider the main nebula's shape (Schwarz et al. 1992). If we were seeing a homogeneous shell expanding at a fixed velocity, we would expect to detect a roughly elliptical slit spectrum (Pottasch 1984, p. 128) and only two components. According to Marten, Gęsicki, & Szczerba (1992), the segregation effect at different velocities within the shell is due to the propagation of an ionization front through it. Newly ionized material increases its pres-

TABLE 2

VELOCITIES OF THE SHELLS

Region	Emission Line	Component	V_{LSR} (km s^{-1})
Main Nebula.....	[N II] λ6583	1	10.6 ± 0.3
		2	26.14 ± 0.15
		3	49.75 ± 0.22
		4	62.96 ± 0.15
	Hα λ6563	1	19.2
		2	23.3
		3	36.3
		4	45.3
Halo	[N II] λ6583	1	30.9 ± 2.3
		2	45.6 ± 2.2

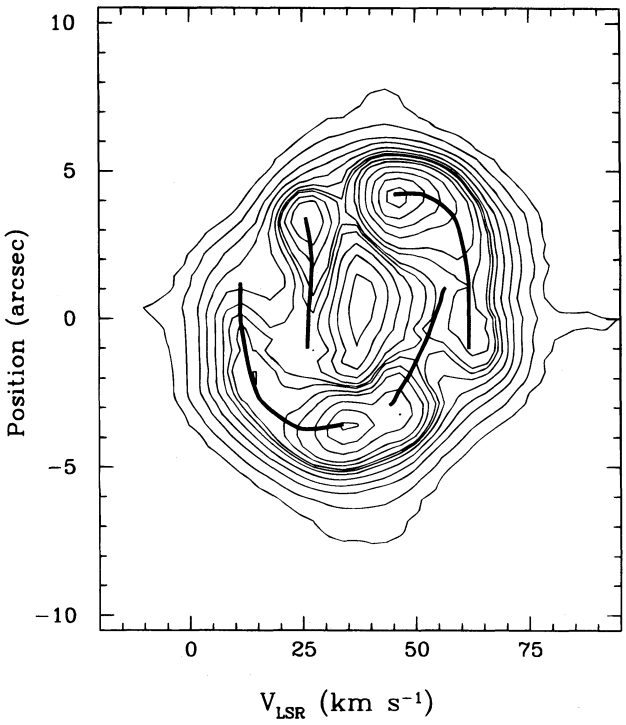

FIG. 4.—Contour map of the position-velocity plot of the main nebula obtained from the [N II] λ6584 line. A tentative fit was made to the different components (*solid lines*) over the contours.

sure and accelerates the outer material near the ionization front, decelerating the iner nebular parts. Figure 4 shows a position-velocity plot of the main nebula in the form of a contour map of the [N II] λ6584 line and clearly confirms the presence of different kinematical components. However, the asymmetry of the spatial distribution of the velocity components does not match the idea of two spherical shells expanding at different velocities. The behavior observed is qualitatively consistent with the radiative gasdynamic models of aspherical PNs presented by Frank & Mellema (1994; see Figs. 4 and 5 at inclination 45°) which consider the interaction of a tenuous fast wind with an aspherical superwind. The observed morphology and kinematics indicate that, even though M1-46 displays some asphericity, departure from sphericity is lower than that of Frank & Mellema's model A.

We also compute the velocities from the Hα line, which appear lower [V_{exp}(H I) ~ 13 km s^{-1}; see Table 2] than those derived from the [N II] λ6584 line. Although the velocity values deduced from the Hα line are more uncertain due to the higher thermal broadening that affects this line, the well-known effect (e.g., Weinberger 1989) that the largest expansion velocity occurs in the lowest ionization stage is seen in M1-46. Meatheringham et al. (1988) calculated an expansion velocity of 7 km s^{-1} from the [O III] λ5007 line, although, due to the lower spectral resolution that they used (~11.5 km s^{-1}), they did not resolve the two velocity components. Figure 2 shows that the nebular Hα emission is superimposed on a broad feature (270 km s^{-1}) associated with the central star.

The expansion velocity of the halo has been inferred from the [N II] line. Two components are detected just on the edge of the main nebula (Table 2). After correcting for geometrical projection, the halo expansion was estimated to be 8 ± 1.6 km s^{-1}.

4. PHYSICAL CONDITIONS AND ABUNDANCES IN M1-46

4.1. *Extraction of the One-dimensional Spectra*

With the aim of determining the spatial extent of the different nebular regions, we examined the spatial profiles of different lines (Hα, [O III] λ5007, [N II] λ6584, [S II] λλ6717, 6731, and He II λ4686), extracted from the low-dispersion two-dimensional spectra. The extracted one-dimensional spectra correspond to the following regions: the one in the direction of the nucleus (N); another describing the main nebula (M); and final one corresponding to the halo (H). The locations of these spectra are labeled against the [N II] λ6584 surface brightness profile in Figure 5. The spatial extension is 3″ for region N and 10″ for region M. For region H, we also added the contribution from the longer exposure long-slit spectrum obtained with an offset of 13″ from the central star. The spectra are shown in Figure 6, with the blue and red parts presented separately. The spectral region which contains the Hα, [N II], and [S II] lines has been enlarged and appears in the right panels. The spectrum of the central star is examined in more detail in § 4.3.

The interstellar extinction constant, c_β, was determined from the Balmer decrement (Hα, Hβ, and Hγ lines) in the main nebula, since this spectrum has the highest signal-to-noise ratio. We derived $c_\beta = 0.70 \pm 0.04$, which is the average of the extinction values calculated from the Hα/Hβ and Hα/Hγ ratios. No evidence of self-absorption in Hβ was found. The Hα/Hβ ratio in the other regions suggest higher extinction, but the errors are also higher there. Our value is lower than the value $c_\beta = 1.1$ given by Acker et al. (1992), but these data could be affected by blending in the Hα and [N II] lines. The intrinsic line strengths, which were obtained using the standard reddening law by Whiteford (1958), are shown in Table 3 scaled to an arbitrary value of 100 for the Hβ line intensity. The error estimate includes the line measurement error plus the uncertainty in c_β.

4.2. *Electron Density, Temperature, and Chemical Abundances*

The [S II] λ6731/λ6717 line ratio was used to determine the electron density (N_e), while the electron temperature (T_e) was calculated from the [N II] (λ6584 + λ6548)/λ5755 line ratio. The derived electron densities and temperatures are listed in Table 4.

In region N, the plasma diagnostic was very unreliable due to the weakness of the [S II] and [N II] λ5755 lines. Therefore, we assumed the same values of N_e and T_e as those obtained in the main nebula (region M), where the strength of diagnostic lines allowed an accurate determination. The values that we chose were within the estimate for the physical plasma parameters from the line measurements corresponding to region N. In region H, only N_e was computed, while T_e was set equal to the corresponding value in region M. Despite the uncertainty, the $N_e(400^{+400}_{-230}$ cm^{-3}) in region H is an order of magnitude lower than in region M (~4000 cm^{-3}).

The ionic abundances were computed from the line strengths using a program that solves statistical equilibrium equations for a five-level atom. These values are listed in Table 4. In region M (main nebula), the errors affecting the

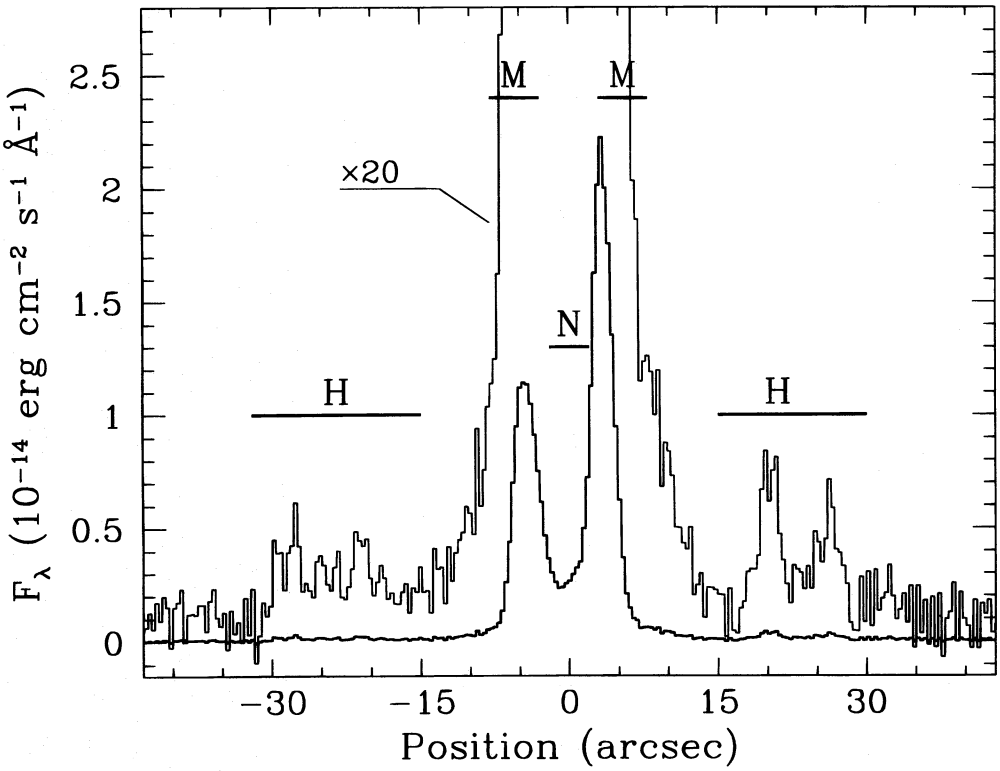

FIG. 5.—Surface brightness profile of the [N II] λ6584 line (*thick line*) extracted from the low-dispersion spectra. The slit is passing through the central star. The effective slit positions for the extracted spectra are labeled over the profile. The same profile multiplied by 20 is also shown (*thin line*) to reveal the fainter outer halo.

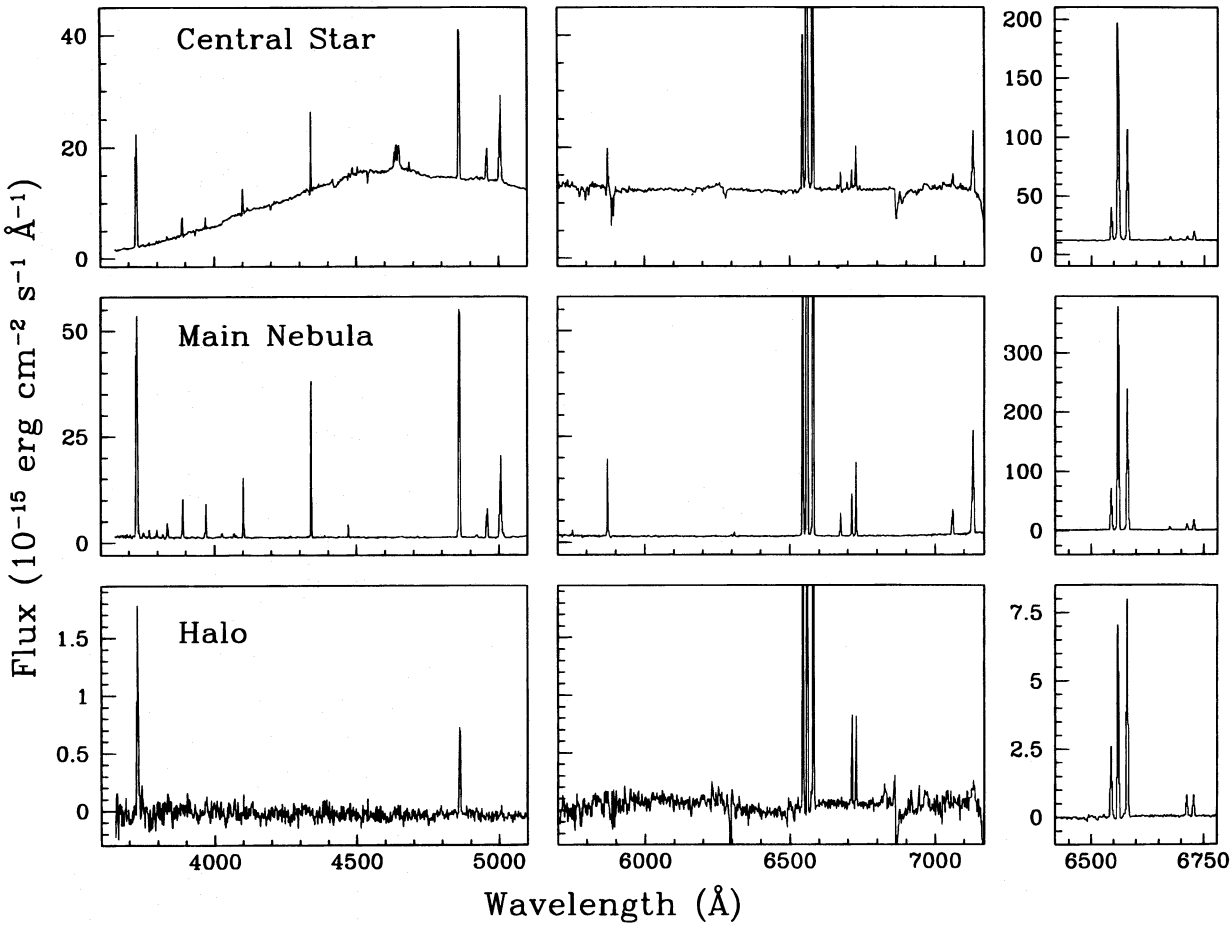

FIG. 6.—Low-resolution spectra of M1-46. Blue and red parts of the spectra are presented separately, as well as the Hα, [N II], and [S II] spectral region conveniently enlarged to reveal the relative intensities of these lines. Each region has been labeled according to the text.

TABLE 3

DEREDDENED LINE INTENSITIES

Line	$f(\lambda)$	Nucleus (N)	Main Nebula (M)	Halo (H)
[O II] λ3727	0.265	115. ± 3.	145. ± 4.	352. ± 22.
H12 λ3750	0.259	...	2.2 ± 0.3	...
H11 λ3770	0.253	0.9 ± 0.1	3.8 ± 0.4	...
H10 λ3797	0.246	...	4.4 ± 0.4	...
He I λ3820	0.241	...	1.3 ± 0.2	...
H9 λ3835	0.236	1.9 ± 0.4	6.2 ± 0.3	...
H8 + He I λ3888	0.223	10.0 ± 0.6	15.2 ± 0.4	...
He + [Ne III] + He I λ3969	0.203	5.8 ± 0.7	13.9 ± 0.4	...
He I λ4026	0.189	...	2.0 ± 0.2	...
[S II] λ4070	0.179	...	1.6 ± 0.2	...
Hδ λ4101	0.172	13.8 ± 0.7	23.2 ± 0.6	...
[C II] λ4267	0.141	...	0.4 ± 0.1	...
Hγ λ4340	0.129	24.4 ± 0.5	42.9 ± 0.2	...
He I λ4388	0.120	...	0.5 ± 0.1	...
He I λ4471	0.095	0.8 ± 0.5	4.5 ± 0.2	...
He II λ4686	0.042	4.1 ± 0.7	...	...
Hβ λ4861	0.000	100.0	100.0	100.0
He I λ4921	−0.015	...	2.0 ± 0.3	...
[O III] λ4959	−0.023	19.7 ± 0.9	12.2 ± 0.6	...
[O III] λ5007	−0.034	59.7 ± 1.4	37.7 ± 0.8	...
He I λ5016	−0.038	...	1.8 ± 0.2	...
λ5700	−0.182	25.3 ± 1.2	...	...
[N II] λ5755	−0.191	1.4 ± 1.0	1.4 ± 0.1	...
He I λ5876	−0.216	13.7 ± 1.0	15.3 ± 0.4	...
[O I] λ6300	−0.285	...	0.3 ± 0.1	...
[S III] + He II λ6312	−0.287	...	0.7 ± 0.1	...
[N II] λ6548	−0.321	38.4 ± 1.7	45. ± 2.	126. ± 16.
Hα λ6563	−0.323	302. ± 12.	277. ± 10.	335. ± 38.
[N II] λ6584	−0.326	133. ± 5.	155. ± 5.	384. ± 45.
He I λ6678	−0.338	4.6 ± 0.4	3.7 ± 0.2	...
[S II] λ6717	−0.343	4.3 ± 0.6	6.4 ± 0.3	37. ± 6.
[S II] λ6731	−0.345	11.5 ± 0.9	10.9 ± 0.4	34. ± 5.
He I λ7065	−0.383	5.1 ± 1.0	5.0 ± 0.3	...
[Ar III] λ7135	−0.391	22.5 ± 1.5	22.8 ± 1.0	...
He I λ7281	−0.406	4.4 ± 1.2	...	...
[O II] λ7320	−0.410	14.2 ± 2.7	13.6 ± 0.7	...
$F(H\beta)$[a]		77.3	159.5	2.14

[a] Dereddened flux in units of 10^{-14} ergs cm^{-2} s^{-1}.

abundances were estimated by taking into account the errors in the line strengths and in the electron densities and temperatures. The helium abundances were corrected for collisional effects (Clegg 1987).

TABLE 4

PHYSICAL CONDITIONS AND CHEMICAL ABUNDANCES

	Nucleus (N)	Main Nebula (M)	Halo (H)
N_e [S II]	4000[a]	4000 ± 450	400^{+400}_{-230}
T_e [N II]	8000[a]	7900 ± 150	8000[a]
$O^{++}/H^+ \times 10^6$	5.0	3.60 ± 0.07	...
$O^+/H^+ \times 10^6$	20.6	28.5 ± 4.	41.
$O^0/H^+ \times 10^6$	...	1.7 ± 0.7	...
$O/H \times 10^6$	26.4	32.3	>41.
$N^+/H^+ \times 10^5$	5.05	6.1 ± 0.5	13.9
$N/H \times 10^5$	6.6	6.8	>13.9
$S^+/H^+ \times 10^7$	11.5	13.1 ± 0.2	32.6
$S/H \times 10^7$	72.	80.	185
$Ar^{++}/H^+ \times 10^6$	3.7	4.13 ± 0.04	...
$Ar/H \times 10^6$	6.9	7.7	...
He^+/H^+ (5876)	0.096	0.107 ± 0.003	...
He^+/H^+ (6676)	0.104	0.840 ± 0.003	...
HE^{++}/H^+ (4686	0.005	...	...
He/H	0.105	0.096 ± 0.012	...
N^+/O^+	0.25	$0.21^{+0.04}_{-0.04}$	0.34
N^+/S^+	44.	46.	43.

[a] Assumed values.

The elemental abundances, calculated by using the ionization correction factors from Kingsburgh & Barlow (1994), are also listed in Table 4. Within errors, chemical abundances do not seem to change from region N to M. The main body of M1-46 appears then to be a type II PN, with low helium enrichment (He/H ~ 0.10) and low nitrogen-to-oxygen ratio (N/O ~ 0.22). The oxygen abundance is half the solar abundance, and the nitrogen abundance is also lower than solar. The ratio Ar/O is 5 times the solar ratio.

As noted above, it was not possible to derive the T_e in the halo due to the scarcity of diagnostic lines assuming the same T_e (8000 K) as in region M, chemical abundances of nitrogen, oxygen, sulphur, and the N/O ratio, were estimated. Those values, higher than those in the inner shell, must be taken as tentative due to the uncertainty in T_e. If the temperature were higher than assumed, as it seems to be the case in the halos of PNs (Middlemass, Clegg, & Walsh 1989; Manchado & Pottasch 1989), abundances should be lower and would be in accordance with the observed abundances at the main nebula.

4.3. *Analysis of the Spectrum of the Central Star*

The spectrum of the central star of M1-46 is shown in Figure 7. The dominant features are N III λλ4634, 4640,

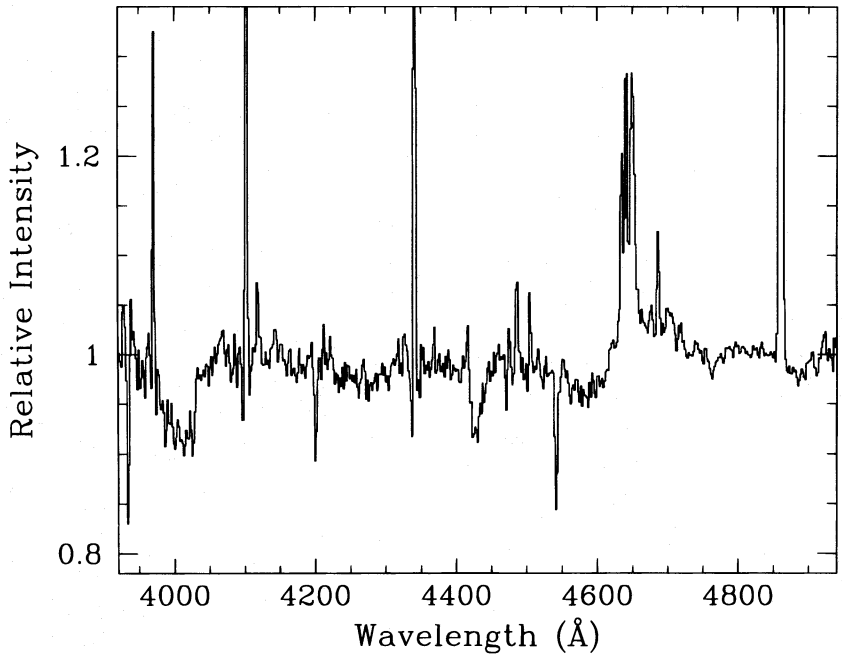

FIG. 7.—Stellar spectrum in the spectral region from 4000 to 4900 Å. The stellar continuum has been normalized to unity. Stellar features are N III λλ4634, 4640, 4641 and H II λ4686 in emission, and He II λλ4542, 4200, and He I λ4471 in absorption, as well as broad absorption wings in the Balmer lines.

4641 and He II λ4686 emissions. The other He II lines are in absorption. The hydrogen spectrum is contaminated by strong nebular lines (out of scale in Fig. 7), but the absorption wings of Hγ and Hδ are visible (the nebular emission in Hβ is too strong, and the photospheric absorption is probably weaker than for the higher members of the Balmer series). Thus, following Méndez, Herrero, & Manchado (1990), the star may be classified as Of. A weak He I λ4471 feature, uncontaminated by nebular emission, seems to be present. No other He I lines are visible.

We have analyzed the spectrum by means of non-LTE plane-parallel models of H and He. This method of analysis

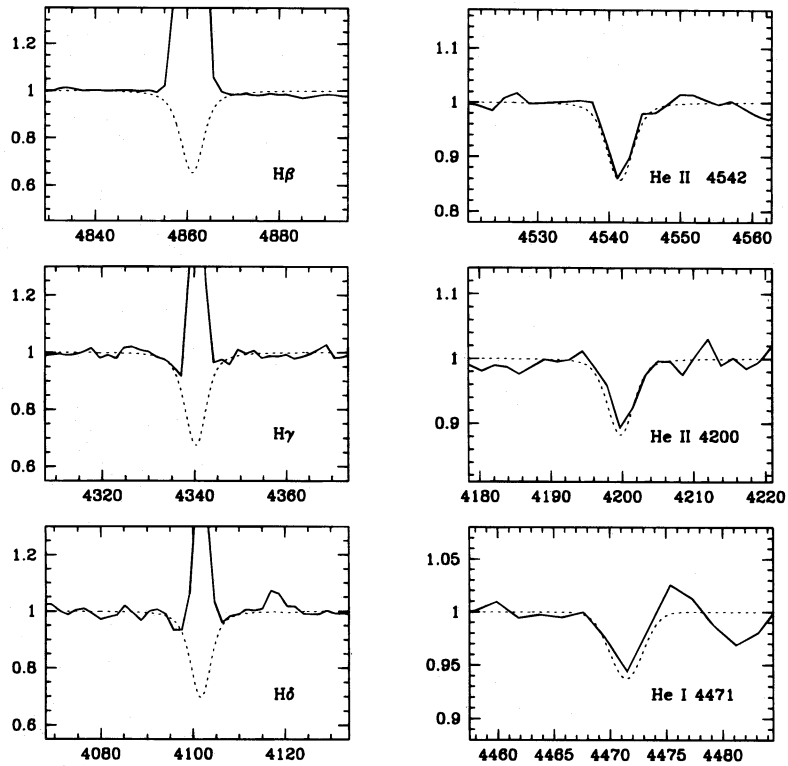

FIG. 8.—Final model fits (*dotted lines*) to the observed stellar H and He absorption profiles. The physical parameters derived are $T_{\rm eff}$ = 45,000 K, log g = 3.7, and $\epsilon = N(\mathrm{He})/[N(\mathrm{H}) + N(\mathrm{He})] = 0.09$. We have adopted a projected equatorial rotational velocity of 80 km s^{-1}.

was described by Herrero et al. (1992). Basically, the temperature is derived from the helium ionization equilibrium, the gravity from the wings of the Balmer lines, and the helium abundance from the absolute absorptions of the He lines. However, the three parameters are related, so that the mentioned fits cannot be made independently.

Following that method, we determined the physical parameters of the central star, $T_{\rm eff} = 45{,}000$ K, $\log g = 3.7$, and $\epsilon = N({\rm He})/[N({\rm H}) + N({\rm He})] = 0.09$, i.e., solar abundance. The quality of the spectrum does not allow us to give precise error bars, and we prefer here to set broad limits to the parameters based on the appearance of the spectrum. We have broadened the profile with a rotational velocity of 80 km s^{-1} (see Méndez et al. 1988), although the broadening is probably due in part to some kind of atmospheric macroturbulence. The temperature has been determined assuming that the identification of the weak He I λ4471 line is correct. However, due to the importance of the temperature determination in our study, we discuss the possible limits for this determination.

The temperature should not be lower than 40,000 K because otherwise the He I lines would be clearly visible, whereas the predicted He II lines would be too weak. This situation cannot be changed by the small correction in gravity needed to fit the Hγ wings at a lower $T_{\rm eff}$, nor can it be modified by varying the helium abundance, because the He I and He II lines would have to vary in opposite directions to fit the observations.

The situation is somewhat different at higher temperatures because here the identification of the He I becomes very important. If this line is not present, we do not have a diagnostic for the ionization equilibrium, and when fitting the He II lines we could compensate for a change in the temperature with a change in the helium abundance (the gravity being fixed at a given temperature by the Balmer wings). At solar helium abundances, the temperature should not exceed 50,000 K because on the contrary the He II lines would be too strong. We could then try to go above 50,000 K by reducing the helium abundance. At the same time, we would have to increase the gravity a little to fit the Balmer wings. But at temperatures above 50,000 K, we should see the N V lines at 4603 and 4619 Å (see the spectra of NGC 6826 and IC 3568 in Méndez et al. 1990). We could assume again that the nitrogen abundance is also lower than solar, but then we would not be able to explain the presence of the N III emission.

In addition to the semiqualitative arguments given above, the adopted parameters are compatible with all the features we observe in the spectrum, in particular with the observed He I, He II, and H lines. The final fits for Hβ, Hγ, Hδ, He I λ4471, He II λ4200, and He II λ4542 are given in Figure 8.

5. DISTANCE AND DYNAMICAL AND EVOLUTIONARY TIMESCALES

The determination of the distance to M1-46 affects both the dynamical time calculations and the position of the central star on the H-R diagram, which is used to derive the interpulse time lap and the stellar mass. Unfortunately, the distance to a PN is one of the most difficult parameters to obtain with any degree of certainty. Hence, we calculate the distance according to the different methods available, namely, the modified Shklovsky statistical distance (Cahn, Kaler, & Stanghellini 1992), the radial velocity of the nebula, the spectroscopic distance, and via the equivalent widths of the sodium ($\lambda\lambda$5890–96) lines (Allen 1976, p. 266). The distance calculated using the statistical method, adopting the diameter of the brightest, innermost shell, amounts to $d = 4.8$ kpc. Using the rotational curve of the Galaxy by Sellwood & Sanders (1988) and assuming circular orbits, we derive a kinematic distance of 4.4 kpc from the radial velocity of M1-46 ($V_{\rm LSR} = 37$ km s^{-1}). Having obtained the atmospheric parameters of the central star and its magnitude, we are in a position to derive the distance to the nebula following the procedure described in Méndez et al. (1988). The distance found was 3.7 kpc. Finally, from the equivalent widths of the sodium lines ($W = 2.186$ Å), we infer $d = 4.4$ kpc, according to Allen's (1976) expression

$$d = 2.0W \, . \qquad (1)$$

The four determinations are in excellent agreement with each other, the differences being lower than 15% of the average value. We adopt $f = 4.4$ kpc in the following calculations.

The dynamical age of a thin PN can be evaluated by dividing the nebular radius by the expansion velocity. Therefore, it is assumed that the expansion velocity is constant. This is true if a steady fast wind is driven into a previous slow wind with an r^{-2} density profile (García-Segura & Mac Low 1995). This is not likely the case of the main nebula, and Mellema's (1993) calculations, including radiative phenomena, suggest that the expansion of PNs does not proceed very uniformly. As regard the halo, it is expanding in a constant density medium, the interstellar medium (ISM) (M1-46 Galactic latitude is $\sim 2°$). If there is not radiation, the expansion law is the one given by Steigman, Strittmatter, & Williams (1975), $v_{\rm exp} \propto t^{1/2}$. However, when the wind density is much larger than the ISM density at the interaction region, the wind is not decelerated by the ISM, and it follows a free expansion law with constant velocity. This is the case of the AGB wind. When the main nebula begins to be optically thin, the radiation is turned on, and the AGB wind and its shell can be accelerated by the thermal pressure of the H II region. At this point there are no analytical solutions or numerical simulations to this problem. Therefore, our results have to be taken as a first approximation until further work is devoted to this hydrodynamical problem.

Knowing the distance, the linear radius is computed from the angular radius, measured over the spatial profile of the [N II] λ6583 line. The expansion velocity of the halo, $V_{\rm exp} = 8.0 \pm 1.6$ km s^{-1} means a dynamical age of 77,000 $\pm$ 15,400 yr. In the main nebula, two different expansion velocities were computed (26.2 and 11.8 km s^{-1}). Assuming that they represent material accelerated and decelerated, respectively

TABLE 5

MASSES AND MASS-LOSS RATE OF THE MAIN NEBULA[a]

Diameter	Linear Size (pc)	Mass ($M_\odot$)	$V_{\rm exp}$ (km s^{-1})	Dynamical Age (yr)	$\dot{M}$ ($M_\odot$ yr^{-1})
14″.4.....	0.307	0.072	26.2	5700	1.3×10^{-5}
			11.8	12650	5.7×10^{-6}

[a] $d = 4.4$ kpc.

(as discussed in § 3), the real expansion velocity of the shell should be between these two values, and in turn the dynamical age should be between 5700 and 12,700 yr. For clarity, we list these parameters in Table 5. We will set the average value, taking the error to be half the difference between the extreme values (9200 $\pm$ 3500 yr). Finally, the time lap between the outer and the inner shell, calculated as the difference between their dynamical ages, is $\Delta t_{\rm dyn} = 6.8 \pm 1.9 \times 10^4$ yr. We must note that most of the uncertainty in $\Delta t_{\rm dyn}$ is caused by the determination of the expansion velocity of the faint halo.

The luminosity of the central star of M1-46 is determined from the V magnitude and the distance. We use the interpolation of the data by Code et al. (1976) and Bohm (1968) (see also the corrections given in Schönberner 1983) to obtain the bolometric correction at 45,000 K, and with $V = 12.83$ (Acker et al. 1992), we derive $\log L/L_\odot = 3.73$. This means a maximum AGB luminosity of $\log L/L_\odot = 3.74$ (Vassiliadis & Wood 1994). Using expression (5) in Frank et al. (1994), this luminosity value corresponds to a theoretical interpulse time lap of approximately 7.61×10^4 yr. In order to find the stellar mass, we place the central star of M1-46 on the H-R diagram and derive the appropriate mass with the help of the synthetic P-AGB tracks of Stanghellini & Renzini (1993). We arrive at $M = 0.6\ M_\odot$, which, according to VW93, corresponds to a progenitor of initial mass $1\ M_\odot$. The chemical abundances found, typical of a type II PN, agree with the mass value reported.

The difference between the interpulse time lap and the dynamical intershell time lap is within the errors, placing this object within the range of stars that have experienced two mass-loss episodes at the TP-AGB.

6. NEBULAR MASS AND MASS-LOSS RATES

Table 5 also includes an estimate of the mass of each shell using expression (V.7) from Pottasch (1984):

$$M(M_\odot) = 11.06 F(\mathrm{H}\beta) t^{0.88} d^2 N_e^{-1}\ , \qquad (2)$$

where $F(\mathrm{H}\beta)$ is the flux in units of 10^{-11} ergs cm^{-2} s^{-1}, d is the distance in kpc, $t = T_e/10{,}000$ K, and N_e is the electron density in cm^{-3}. To apply this expression, we need to know the total Hβ flux from each region. In the case of the main nebula, we studied the spatial profile of the Hβ line in the slit over this region and constructed a surface brightness density function of the Hβ flux ($f_{\mathrm{H}\beta}$) depending only on the radial distance on the sky (θ) to the center of the nebula, i.e., assuming that it does not depend on the angular component (ϕ). This function, with units of flux arcsec^{-2}, was then integrated over the whole surface of the main nebula

$$F(\mathrm{H}\beta) = \int_0^{2\pi} \int_0^R \theta f_{\mathrm{H}\beta}(\theta) d\phi\, d\theta\ , \qquad (3)$$

where R is the angular radius of the main nebula (7.″2). As $f_{\mathrm{H}\beta}$ does not depend on ϕ,

$$F(\mathrm{H}\beta) = 2\pi \int_0^R \theta f_{\mathrm{H}\beta}(\theta) d\theta\ , \qquad (4)$$

which yields $F(\mathrm{H}\beta) = 1.31 \times 10^{-11}$ ergs cm^{-2} s^{-1}, and a total ionized mass of $0.072\ M_\odot$.

According to the previous discussion on the expansion velocity of the main nebula, the averaged mass-loss rate (MLR) is between 5.7×10^{-6} and $1.3 \times 10^{-5}\ M_\odot$ yr^{-1}.

As noted above, the central star's mass of $0.6\ M_\odot$ would correspond to a $1\ M_\odot$ progenitor, which experienced a final mass-loss episode of $0.32\ M_\odot$ at an average rate of $6.4 \times 10^{-6}\ M_\odot$ yr^{-1} during $\sim$50,000 yr (VW93). This mass-loss rate is consistent with the one derived by us. However, the lifetime that we derived for the main nebula, corresponding to this last mass-loss episode, is over 4 times smaller. It is worth noting that the VW93 models, as all the results on post-AGB evolution, depend strongly on the mass-loss treatment. For example, Blöcker (1995) used a modification of Bowen's (1988) mass-loss rate and found rather different lifetimes (see Blöcker's Table 4). Another likely answer to this question is the possibility that the main nebula is ionization bounded, and therefore only a fraction of the mass can be detected. In that case, we would expect to detect molecular emission around the main nebula.

7. SUMMARY

An accurate analysis of new observations of the multiple-shell planetary nebula M1-46 demonstrates that the nebular shells could very well originate from mass loss during the TP-AGB, since the timing of the dynamical evolution of the two shells and the stellar parameters are very much in agreement with each other. The investigation takes into account the velocities of the two shells, the distance to the nebula, the plasma diagnostic analysis, and the spectrum, mass, magnitude, and luminosity of the central star. Further data are needed to conduct an improved abundance analysis, while more observations and analyses of planetary nebulae with similar morphologies are underway, to strengthen the generalization of the results shown here and in Stanghellini & Pasquali (1995).

Despite the main nebula's simple, round shape, the spatially resolved high spectral resolution study has revealed the presence of different kinematical components which cannot be characterized by a single expansion velocity in the scheme of a homogeneous expanding shell. Hydrodynamical calculations offer a qualitative explanation. The different velocities measured in the expanding shell result from the propagation of an ionization front which accelerates the outer material (forward shock) and decelerates the inner parts (reverse shock). In addition, the interaction of an aspherical slow wind with the current fast wind should be considered to account for the main nebula's deviation from sphericity.

The present work proves that the velocity structure of PNs can only be resolved with very high spectral resolution (≤ 7 km s^{-1}). This is an essential point if we want to interpret correctly the observed velocities and obtain a reliable estimate of the dynamical age of each shell.

This work is based partially on observations made with the WHT telescope, operated on the island of La Palma by the Royal Greenwich Observatory in the Spanish Observatorio del Roque de Los Muchachos of the Instituto de Astrofísica de Canarias. This research was funded in part through grant PB90-0570 from the Dirección General de Investigación Científica y Técnica of the Spanish Ministerio de Educación y Ciencia.

REFERENCES

Acker, A., Marcout, J., Ochsenbein, F., Stenholm, B., Tylenda, R., & Schohn, C., ed. 1992, The Strasbourg-ESO Catalogue of Galactic Planetary Nebulae, Part II (Munich: European Southern Observatory), 118
Allen, C. W. 1976, Astrophysical Quantities (3d ed.; London: Athlone)
Balick, B., Gonzalez, G., Frank, A., & Jacoby, G. 1992, ApJ, 392, 582
Blöcker, T. 1995, A&A, 297, 727
Böhm, K. H. 1968, in IAU Symp. 34, Planetary Nebulae, ed. D. E. Osterbrock & C. R. O'Dell (Dordrecht: Reidel), 297
Bowen, G. H. 1988, ApJ, 329, 299
Cahn, J. H., Kaler, J. B., & Stanghellini, L. 1992, A&AS, 94, 399
Chu, Y.-H., Jacoby, G. H., & Arendt, R. 1987, ApJS, 64, 529
Clegg, R. E. S. 1987, MNRAS, 229, 31p
Code, A. D., Bless, R. C., Davis, J., & Brown, R. H. 1976, ApJ, 203, 417
Frank, A., Balick, B., & Riley, J. 1990, AJ, 100, 1903
Frank, A., & Mellema, G. 1994, ApJ, 430, 800
Frank, A., van der Veen, W. E. C. J., & Balick, B. 1994, A&A, 282, 554
García-Segura, G., & Mac Low, M. 1995, ApJ, 455, 145
Herrero, A., Kudritzki, R. P., Vilchez, J. M., Kunze, D., Butler, K., & Haser, S. 1992, A&A, 261, 209
Kingsburgh, R. L., & Barlow, M. J. 1994, MNRAS, 271, 257
Manchado, A., & Pottasch, S. R. 1989, A&A, 222, 219
Marten, H., Gęsicki, K., & Szczerba, R. 1992, in IAU Symp. 155, Planetary Nebulae, ed. R. Weinberger & A. Acker (Dordrecht: Kluwer), 315
Meatheringham S. J., Wood, P. R., & Faulkner, D. J. 1988, ApJ, 334, 862
Mellema, G. 1993, Ph.D. thesis, Leiden Univ.
Méndez, R. H., Herrero, A., & Manchado, A. 1990, A&A, 229, 152
Méndez, R. H., Kudritzki, R. P., Herrero, A., Husfeld, D., & Groth, H. G. 1988, A&A, 190, 113
Middlemass, D., Clegg, R. E. S., & Walsh, J. R. 1989, MNRAS, 239, 1
Pottasch, S. R. 1984, Planetary Nebulae (Dordrecht: Reidel)
Schwarz, H. E., Corradi, R. L. M., & Melnick, J. 1992, A&AS, 96, 23
Schönberner, D. 1983, A&A, 79, 108
Sellwood, J. A., & Sanders, R. H. 1988, MNRAS, 233, 611
Stanghellini, L., & Pasquali, A. 1995, ApJ, 452, 286
Stanghellini, L., & Renzini, A. 1993, in IAU Symp. 155, Planetary Nebulae, ed. R. Weinberger & A. Acker (Dordrecht: Kluwer), 473
Steigman, G., Strittmatter, P. A., & Williams, R. E. 1975, ApJ, 198, 575
Vassiliadis, E., & Wood, P. R. 1993, ApJ, 413, 641 (VW93)
———. 1994, ApJS 92, 125
Weinberger, R. 1989, A&AS, 78, 301
Whitford, A. E. 1958, AJ, 63, 201